Eur. Phys. J. A **25**, 345–354 (2005)
DOI 10.1140/epja/i2005-10131-2

THE EUROPEAN PHYSICAL JOURNAL A

Rotational structures in ^{123}Cs

Kuljeet Singh[1], Z. Naik[2], R. Kumar[1], J. Goswamy[1], D. Mehta[1], N. Singh[1,a], C.R. Praharaj[2], E.S. Paul[3], K.P. Singh[1], R.P. Singh[4], S. Muralithar[4], N. Madhavan[4], J.J. Das[4], S. Nath[4], A. Jhingan[4], P. Sugathan[4], and R.K. Bhowmik[4]

[1] Department of Physics, Panjab University, Chandigarh 160 014, India
[2] Institute of Physics, Bhubaneswar 751 005, India
[3] Oliver Lodge Laboratory, University of Liverpool, Liverpool, L69 7ZE, UK
[4] Nuclear Science Centre, Aruna Asaf Ali Marg, New Delhi 110 067, India

Received: 20 April 2005 / Revised version: 13 July 2005 /
Published online: 5 October 2005 –
Communicated by D. Schwalm

Abstract. High-spin states in ^{123}Cs, populated via the ^{100}Mo (^{28}Si, p4n) fusion-evaporation reaction at $E_{\rm lab}$ = 130 MeV, have been investigated employing in-beam γ-ray spectroscopic techniques. Rotational bands, built on $\pi g_{7/2}$, $\pi g_{9/2}$ and the unique-parity $\pi h_{11/2}$ orbitals, have been extended and evolve into bands involving rotationally aligned $\nu(h_{11/2})^2$ and $\pi(h_{11/2})^2$ quasiparticles. A three-quasiparticle band based on the high-K $\pi h_{11/2} \otimes \nu g_{7/2} \otimes \nu h_{11/2}$ configuration has also been observed. Total Routhian Surface (TRS) calculations have been used to predict the nuclear shape parameters (β_2, β_4, γ) for the various assigned configurations. The assigned configurations have been discussed in the framework of a microscopic theory based on the deformed Hartree-Fock (HF) and angular-momentum projection techniques.

PACS. 21.10.Re Collective levels – 23.20.Lv γ transitions and level energies – 21.60.-n Nuclear structure models and methods – 27.60.+j $90 \leq A \leq 149$

1 Introduction

Spectroscopic studies of nuclei in $A \sim 125$ mass region continue to be a focus of attention due to the multiplicity of shapes and a richness of nuclear-structure phenomena. These nuclei are characterised with a γ-soft deformed core. Theoretical calculations predict a variety of minima in the nuclear potential energy surface, and indeed experimentally low-deformation minima are found to coexist with oblate, triaxial or highly deformed minima [1,2]. The occurrence of high-Ω orbits near the proton and neutron Fermi surfaces of these nuclei leads to high-K configurations and isomers. In the odd-Z even-N nuclei, the shape at low rotational frequencies is mainly influenced by the valence quasiproton. It is of interest to track the $\pi h_{11/2}$ and $\pi g_{9/2}$ bands in this mass region with the position of proton and neutron Fermi surfaces to understand their respective deformation-driving tendencies. At higher frequencies additional rotationally aligned $h_{11/2}$ quasineutrons/protons compete to polarise the γ-soft core. Maximally spin aligned states have been observed in various Sb, Te, I, Xe and La isotopes. Triaxial deformation in this mass region has been inferred from the observed rotational-alignment frequencies, staggering behaviour, $M1$ reduced transition probabilities and chiral twin bands. The extension of systematics of chiral bands observed in the doubly odd nuclei to the odd-even ^{135}Nd [3] and even-even ^{136}Nd [4] nuclei with multiquasiparticle configuration provides added impetus to investigations in this mass region. Magnetic dipole bands based on configurations involving an aligned $\nu h_{11/2}$ pair have been reported in ^{131}Cs [5] and doubly odd ^{132}Cs [6]. State-of-the-art γ-ray spectrometers consisting of an array of clover and cluster Ge detectors have greatly enhanced the capability to explore details of the bands and interband transitions extending to high spins [7], and have encouraged further investigations of nuclear structure using γ-ray spectroscopic techniques.

The present in-beam gamma spectroscopic investigations have been aimed at looking for the above-mentioned structural features in the ^{123}Cs nucleus. Total Routhian Surface (TRS) calculations and a microscopic model based on the deformed Hartree-Fock (HF) and angular-momentum projection techniques have been used to study the band structures in this nucleus. A short communication showing the level scheme of ^{123}Cs deduced from the present work has previously been reported [8]. Recently, the level structure of ^{123}Cs has been established to higher spins ($\sim 71/2\hbar$) via the ^{64}Ni (^{64}Ni, p4n) reaction using thin target and the Gammasphere spectrometer [9]; that work provides spectroscopic information up to a higher-spin range.

[a] e-mail: nsingh@pu.ac.in

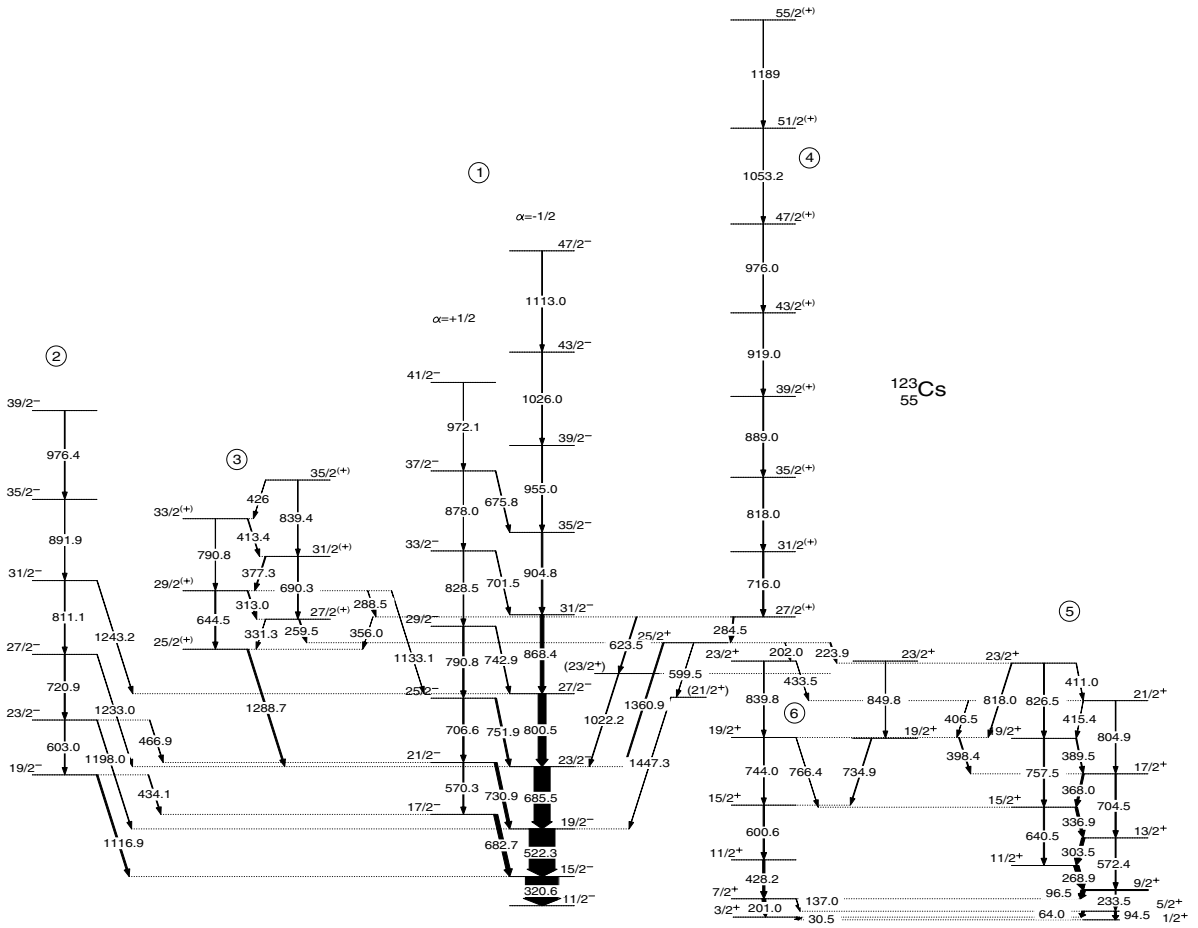

Fig. 1. The level scheme of ^{123}Cs established from the present work.

2 Experimental details and data analysis

The ^{100}Mo(^{28}Si, p4n) fusion-evaporation reaction at 130 MeV was used to populate excited states in the ^{123}Cs nucleus. The experiment was performed using a ^{28}Si beam provided by the 15 UD pelletron accelerator at the Nuclear Science Centre (NSC), New Delhi. The target consisted of a 3 mg/cm^2 thick enriched ^{100}Mo foil backed with a 15 mg/cm^2 thick ^{208}Pb foil to stop the recoiling nuclei. Gamma rays emitted by the evaporation residues were detected using an array consisting of 8 Compton-suppressed clover detectors. Each clover detector consists of four HPGe crystals in a single vacuum housing. The clover detectors were mounted in two groups of four each making angles of ±81° and ±141° with the beam direction, and having an inclination of ±18° with the horizontal plane. The array is called the Indian National Gamma Array (INGA) and was jointly set up by NSC, New Delhi, TIFR, Mumbai, SINP and IUC-DAEF, Kolkata [10]. Each clover was treated as a single detector and data were collected in LIST mode when two or more clovers fired in coincidence within a time window of $2\tau = 200$ ns. A total of 5×10^8 coincidence events were collected in this experiment. The nuclei populated in the reaction were ^{123}Ba (∼ 8%), ^{124}Ba (∼ 25%), ^{125}Ba (∼ 5%), ^{123}Cs (∼ 14%), ^{124}Cs (∼ 12%), ^{125}Cs (∼ 7%), ^{120}Xe (∼ 5%), ^{121}Xe (∼ 10%), and ^{122}Xe (∼ 4%).

In the offline analysis, the recorded coincidence events were sorted into two-dimensional γ-γ matrices using INGASORT [10]. The gains of the Ge detectors were software matched to 0.5 keV/channel before incrementing the matrix. Background-subtracted coincidence spectra were generated and intensity analysis was performed using the computer codes RADWARE [11] and PEAKFIT [12], respectively. The placement of gamma transitions in the level scheme is based upon their coincidence relationships, energy sums and intensities. In order to determine the dipole/quadrupole nature of the gamma transitions, directional correlation (DCO) ratios were extracted using an asymmetric matrix made by sorting data with 141° detectors on one axis and 81° detectors on the other axis. The energies, intensities, DCO ratios and the assigned multipolarities for transitions in ^{123}Cs are given in table 1. Figure 1 depicts the level scheme of ^{123}Cs obtained in the present work. The spin-parity of the ground state ($t_{1/2}$ = 5.9 m) has been adopted from earlier low-spin studies of ^{123}Cs as $J^\pi = 1/2^+$ [13]. The band structures have been labelled 1–6 in order to facilitate the discussion. Band 1 is built on an isomeric state ($t_{1/2} = 1.7$ s, excitation energy = 156 keV) with $J^\pi = 11/2^-$ [13,14]. The spin-parity

Table 1. Gamma-ray energies, intensities, DCO ratios and multipolarities for transitions assigned to ^{123}Cs.

E (keV)[a]	Intensity[b]	DCO ratio	Assigned multipolarity	$I_i^\pi \rightarrow I_f^\pi$
30.5	–	–	–	$3/2^+ \rightarrow 1/2^+$
64.0	–	–	–	$5/2^+ \rightarrow 3/2^+$
94.5	–	–	–	$5/2^+ \rightarrow 1/2^+$
96.5	–	–	$M1$	$9/2^+ \rightarrow 7/2^+$
137.0	73	–	–	$7/2^+ \rightarrow 5/2^+$
201.0	209	1.21 (19)	$E2$	$7/2^+ \rightarrow 3/2^+$
202.0	–	–	–	$25/2^{(+)} \rightarrow 23/2^+$
223.9	20	0.58 (10)	$M1$	$25/2^{(+)} \rightarrow 23/2^+$
233.5	–	–	$E2$	$9/2^+ \rightarrow 5/2^+$
259.5	28	0.60 (8)	$M1$	$27/2^+ \rightarrow 25/2^+$
268.9	141	0.78 (15)	$M1$	$11/2^+ \rightarrow 9/2^+$
284.5	25	0.68 (12)	$M1$	$27/2^{(+)} \rightarrow 25/2^{(+)}$
288.5	9	–	$(M1)$	$29/2^{(+)} \rightarrow 27/2^{(+)}$
303.5	96	0.62 (8)	$M1$	$13/2^+ \rightarrow 11/2^+$
313.0	24	–	–	$29/2^{(+)} \rightarrow 27/2^{(+)}$
320.6	1000	1.06 (8)	$E2$	$15/2^- \rightarrow 11/2^-$
331.3	9	0.60 (12)	$M1$	$27/2^{(+)} \rightarrow 25/2^{(+)}$
336.9	86	0.60 (7)	$M1$	$15/2^+ \rightarrow 13/2^+$
356.0	5	0.60 (12)	$M1$	$27/2^{(+)} \rightarrow 25/2^{(+)}$
368.0	58	0.65 (8)	$M1$	$17/2^+ \rightarrow 15/2^+$
377.3	26	0.51 (10)	$M1$	$31/2^{(+)} \rightarrow 29/2^{(+)}$
389.5	26	0.63 (8)	$M1$	$19/2^+ \rightarrow 17/2^+$
398.4	24 ( )	0.61 (9)	$M1$	$19/2^+ \rightarrow 17/2^+$
406.5	10	–	$M1$	$21/2^+ \rightarrow 19/2^+$
411.0	14	–	$M1$	$23/2^+ \rightarrow 21/2^+$
413.4	17	0.46 (12)	$M1$	$33/2^{(+)} \rightarrow 31/2^{(+)}$
415.4	6	–	$M1$	$21/2^+ \rightarrow 19/2^+$
426.0	6	–	$M1$	$35/2^{(+)} \rightarrow 33/2^{(+)}$
428.2	66	1.14 (16)	$E2$	$11/2^+ \rightarrow 7/2^+$
433.5	10	–	$M1$	$23/2^+ \rightarrow 21/2^+$
434.1	25	0.56 (8)	$M1$	$19/2^- \rightarrow 17/2^-$
466.9	17	–	$M1$	$23/2^- \rightarrow 21/2^-$
522.3	788	1.02 (8)	$E2$	$19/2^- \rightarrow 15/2^-$
570.3	28	0.75 (24)	$E2$	$21/2^- \rightarrow 17/2^-$
572.4	26	1.02 (12)	$E2$	$13/2^+ \rightarrow 9/2^+$
599.5	8	–	$E2$	$25/2^{(+)} \rightarrow (21/2^+)$
600.6	38	1.12 (15)	$E2$	$15/2^+ \rightarrow 11/2^+$
603.0	17	–	$E2$	$23/2^- \rightarrow 19/2^-$
623.5	16	0.83 (20)	$E2$	$27/2^{(+)} \rightarrow (23/2^+)$
640.5	38	0.88 (15)	$E2$	$15/2^+ \rightarrow 11/2^+$
644.5	25	0.87 (20)	$E2$	$29/2^{(+)} \rightarrow 25/2^{(+)}$
675.8	17	–	$M1$	$37/2^- \rightarrow 35/2^-$
682.7	129	0.47 (9)	$M1$	$17/2^- \rightarrow 15/2^-$
685.5	499	0.94 (10)	$E2$	$23/2^- \rightarrow 19/2^-$
690.3	18	–	$E2$	$31/2^{(+)} \rightarrow 27/2^{(+)}$
701.5	17	0.57 (12)	$M1$	$33/2^- \rightarrow 31/2^-$

Table 1. Continued.

E (keV)[a]	Intensity[b]	DCO ratio	Assigned multipolarity	$I_i^\pi \rightarrow I_f^\pi$
704.5	39	0.89 (15)	$E2$	$17/2^+ \rightarrow 13/2^+$
706.6	41	1.04 (15)	$E2$	$25/2^- \rightarrow 21/2^-$
716.0	34	0.95 (10)	$E2$	$31/2^{(+)} \rightarrow 27/2^{(+)}$
720.9	28	0.82 (20)	$E2$	$27/2^- \rightarrow 23/2^-$
730.9	86	0.45 (9)	$M1$	$21/2^- \rightarrow 19/2^-$
734.9	16	0.94 (18)	$E2$	$19/2^+ \rightarrow 15/2^+$
742.9	22	0.47 (7)	$M1$	$29/2^- \rightarrow 27/2^-$
744.0	15	1.12 (18)	$E2$	$19/2^+ \rightarrow 15/2^+$
751.9	43	0.45 (8)	$M1$	$25/2^- \rightarrow 23/2^-$
757.5	36	1.24 (20)	$E2$	$19/2^+ \rightarrow 15/2^+$
766.4	7	–	$E2$	$19/2^+ \rightarrow 15/2^+$
790.8	38	0.93 (15)	$E2$	$29/2^- \rightarrow 25/2^-$
790.8	14	–	$E2$	$33/2^{(+)} \rightarrow 29/2^{(+)}$
800.5	233	0.93 (10)	$E2$	$27/2^- \rightarrow 23/2^-$
804.9	24	1.02 (21)	$E2$	$21/2^+ \rightarrow 17/2^+$
811.1	17	–	$E2$	$31/2^- \rightarrow 27/2^-$
818.0	35	1.06 (20)	$E2$	$35/2^{(+)} \rightarrow 31/2^{(+)}$
818.0	20	–	$E2$	$23/2^+ \rightarrow 19/2^+$
826.5	25	–	$E2$	$23/2^+ \rightarrow 19/2^+$
828.5	16	–	$E2$	$33/2^- \rightarrow 29/2^-$
839.4	19	–	$E2$	$35/2^{(+)} \rightarrow 31/2^{(+)}$
839.8	16	–	$E2$	$23/2^+ \rightarrow 19/2^+$
849.8	10	–	$E2$	$23/2^+ \rightarrow 19/2^+$
868.4	108	0.86 (15)	$E2$	$31/2^- \rightarrow 27/2^-$
878.0	11	–	$E2$	$37/2^- \rightarrow 33/2^-$
889.0	24	0.96 (15)	$E2$	$39/2^{(+)} \rightarrow 35/2^{(+)}$
891.9	14	–	$E2$	$35/2^- \rightarrow 31/2^-$
904.8	50	0.87 (15)	$E2$	$35/2^- \rightarrow 31/2^-$
919.0	18	0.92 (25)	$E2$	$43/2^{(+)} \rightarrow 39/2^{(+)}$
955.0	29	0.84 (15)	$E2$	$39/2^- \rightarrow 35/2^-$
972.1	5	–	$E2$	$41/2^- \rightarrow 37/2^-$
976.0	15	–	$E2$	$47/2^{(+)} \rightarrow 43/2^{(+)}$
976.4	8	–	$E2$	$39/2^- \rightarrow 35/2^-$
1022.2	21	–	$(E1)$	$(23/2^+) \rightarrow 23/2^-$
1026.0	15	–	$E2$	$43/2^- \rightarrow 39/2^-$
1053.2	7	–	$E2$	$51/2^{(+)} \rightarrow 47/2^{(+)}$
1113.0	10	–	$E2$	$47/2^- \rightarrow 43/2^-$
1116.9	52	–	–	$19/2^- \rightarrow 15/2^-$
1133.1	15	0.62 (8)	$E1$	$29/2^+ \rightarrow 27/2^-$
1188.2	4	–	$E2$	$55/2^{(+)} \rightarrow 51/2^{(+)}$
1198.0	20	1.18 (25)	$E2$	$23/2^- \rightarrow 19/2^-$
1233.0	14	0.80 (25)	$E2$	$27/2^- \rightarrow 23/2^-$
1243.2	15	0.77 (25)	$E2$	$31/2^- \rightarrow 27/2^-$
1288.7	45	0.57 (7)	$E1$	$25/2^{(+)} \rightarrow 23/2^-$
1360.9	25	0.70 (12)	$E1$	$25/2^{(+)} \rightarrow 23/2^-$
1447.3	14	–	$(E1)$	$(21/2^+) \rightarrow 19/2^-$

([a]) Energies are accurate to 0.5 keV for strong transitions. The errors increase to 0.7 keV for weaker transitions (relative intensity < 30).
([b]) Error in intensity value is 5–20%.

assignments to various states in bands 1–6 are discussed in our earlier report and agree with those proposed in ref. [9].

The level scheme of ^{123}Cs established prior to this work has been studied by Hughes *et al.* [15] and Lidén *et al.* [16] using ^{108}Pd (^{19}F, 4n) and ^{92}Mo (^{34}S, 3p) reactions, respectively. Previous investigations revealed rotational structures based on the $\pi h_{11/2}$ orbital (band 1), the $\pi h_{11/2}$ orbital coupled to a γ-vibration (band 2), the $\pi g_{9/2}$ orbital (band 5) and the $\pi g_{7/2}$ orbital (band 6). The bandhead energy of the $\pi g_{9/2}$ band differs in these studies [15,16] and that for the $\pi g_{7/2}$band was not known and assigned a tentative bandhead spin-parity $J^\pi = (7/2^+)$. The level scheme inferred from the present work preserves major features of the previously [15,16] and recently established level schemes [9]. The positive-parity band 3 comprises of strong dipole transitions along with weak $E2$ crossover transitions, while band 4 exhibits rotational structure consisting only of $E2$ transitions. The decay patterns of bands 3 and 4 are complex, mostly connecting to the low-lying states with both parities. The transitions in band 4 reported in ref. [9] could be seen up to spin $55/2\hbar$ in the present experiment. Apart from the 1447 keV transition ($63/2^+ \rightarrow 59/2^+$) shown in band 4 in ref. [9], a second 1447 keV transition feeding the $19/2^-$ state is also observed. The bandhead energies of the $\pi g_{9/2}$ (band 5) and $\pi g_{7/2}$ (band 6) bands have been determined on the basis of linking transitions to the low-energy levels observed in the β^+/EC decay of ^{123}Ba ($t_{1/2}$ = 2.7 m) [13] and intensity balance from the present coincidence data. The relevant arguments have been discussed in details elsewhere [8]. The 328.1 keV level has been identified as an isomer and assigned $J^\pi = 9/2^+$ rather than the earlier proposed ($5/2^+$, $7/2^+$) value [13]. Similar conclusions are deduced in the thin-target experiment [9] using Gammasphere spectrometer, where the 97 and 234 keV transitions depopulating the 328 keV level were not observed as the evaporation residues from the recoiling nuclei decay out of the focal plane of the collimated detectors. The $\pi g_{9/2}$ bandhead states are also found to be isomeric in the lighter $_{51}$Sb, $_{53}$I and $_{55}$Cs isotopes. The bandhead energies of the $\pi g_{9/2}$ (band 5) and $\pi g_{7/2}$ (band 6) bands are further well supported by a number of observed interband transitions connecting bands 1, 3, 4 and 5.

3 Results and discussion

The level scheme of ^{123}Cs shows properties typical of a collectively rotating deformed nucleus. Nilsson configuration assignments to various observed bands are based on arguments concerning the band-crossing frequencies, signature splitting, additivity of alignments of the involved quasiparticles and the deduced $B(M1)/B(E2)$ ratios. The alignments (i_x) extracted for different bands (fig. 1) using the Harris parameters [17], $J_o = 17.0\hbar^2$ MeV^{-1} and $J_1 = 25.8\hbar^4$ MeV^{-3}, are shown as a function of rotational frequency in fig. 2. The experimental $B(M1)/B(E2)$ ratios have been calculated using the energies and intensities of $\Delta J = 1$ and 2 transitions for the levels of the strongly coupled bands 3 and 5. The $E2/M1$ mixing ratio (δ) for the $\Delta J = 1$ transitions has been taken as zero. This assumption does not significantly influence the experimental results since the mixing ratio is generally small [18].

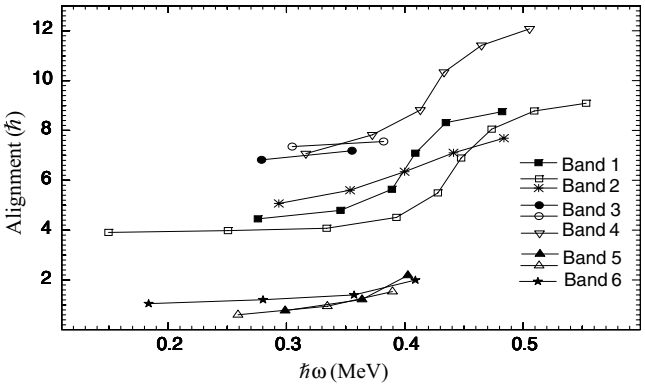

Fig. 2. Experimental alignment plots for bands 1–6 observed in ^{123}Cs.

Band 1 is based on the unique-parity $h_{11/2}$ proton orbital and both the favoured ($\alpha = -1/2$) and unfavoured ($\alpha = +1/2$) signatures are observed. It shows a large initial alignment $\sim 4\hbar$ (fig. 2) and signature splitting ($\Delta e'$) $\sim$ 400 keV at $\hbar\omega = 0.30$ MeV [8]. An alignment of a pair of $h_{11/2}$ neutrons is observed for both the signatures in this band at a frequency of $\hbar\omega \approx 0.43$ MeV with a corresponding alignment gain of $4.5\hbar$ (fig. 2). The signature splitting in the yrast band remains large $\sim$ 200 keV even after the alignment [8], which indicates that the nuclear shape remains close to prolate. The systematics of the neutron alignment frequency in the yrast band of the odd-A $^{119-131}$Cs isotopes has been discussed by Smith *et al.* [19].

Band 2 is identified as the γ-vibrational band built on the favoured signature partner of the $h_{11/2}$ band and is a feature common to nuclei in this mass region. The strongly coupled band 5 has been assigned a $g_{9/2}$ proton hole configuration. The $[404]9/2^+$ component of the $\pi g_{9/2}$ orbital, which originates from below the $Z = 50$ shell closure, becomes energetically favourable at larger prolate deformation. The large positive g-factor 1.27 [20] and high-Ω values are responsible for the observed large $B(M1)/B(E2) \sim 3$ $(\mu_N/\mathrm{eb})^2$ values and near to zero signature splitting. Bands based on the $\pi g_{9/2}[404]9/2^+$ orbital have been observed in the lighter odd-A $^{117-127}$Cs [19,16,21,22] isotopes, but not in ^{129,131}Cs [23, 5] where the deformation reduces to $\beta_2 \sim 0.12$. The other positive-parity band labelled 6 has been assigned the $\pi g_{7/2}$ configuration. This band has interlinking dipole and quadrupole transitions with the high-Ω $\pi g_{9/2}[404]9/2^+$ band. The $\pi h_{11/2}$ and $\pi g_{7/2}$ bands have been observed in the odd-A $^{117,121-133}$Cs isotopes [19,16,21–23,5,24]. The population strength of the $\pi g_{7/2}$ band relative to that of the $\pi h_{11/2}$ band increases considerably with increasing mass number. This happens primarily because the excitation energy of the $h_{11/2}$ level is increasing thus becoming less yrast in the heavier isotopes. These facts are consistent with a decreasing nuclear deformation with increasing

mass. Also, features of the $\pi g_{7/2}$ and $\pi d_{5/2}$ bands become distinctive in the heavier ^{127,129,131,133}Cs isotopes [5,22–24]. In the lighter Cs isotopes, significant admixture of the $\pi d_{5/2}$orbitals has been noticed in the $\pi g_{7/2}$bands [21].

The positive-parity decoupled band 4 shows a large initial alignment $\sim 7.5\hbar$ (fig. 2) indicating it to be based on a three-quasiparticle configuration. Interestingly, the band exhibits an upbend at a rotational frequency of $\hbar\omega \sim 0.42$ MeV with an alignment gain of $4.5\hbar$. The alignment plot for this band is very similar to the one corresponding to band 1 except for the value of initial alignment. So, one is enticed to conclude that the upper observed portion of band 4 is a five-quasiparticle structure involving $(\nu h_{11/2})^2$. This involvement of the $\nu h_{11/2}$ quasiparticle in the initial configuration of band 4 can be ruled out on the basis of blocking arguments. The large value of the initial alignment $\sim 7.5\hbar$ can be accounted for only by the $\pi(h_{11/2})^2$ alignment as the $\pi g_{7/2}$ and $\pi g_{9/2}$ bands exhibit low alignment values ($\sim 1\hbar$). The first $\pi(h_{11/2})^2$ alignment is not blocked in the $\pi g_{9/2}$ or $\pi g_{7/2}$ bands. In the neighbouring isotone ^{124}Ba [25], the $\pi(h_{11/2})^2$ alignment is observed at 0.37 MeV, similar to that observed in the $\pi g_{9/2}$band of ^{123,125}La [26,20]. An alignment gain of $\sim 8\hbar$ was observed for the $\pi(h_{11/2})^2$ alignment in the $\pi g_{7/2}$ band in ^{125}La. The $\pi g_{9/2}\otimes\pi(h_{11/2})^2$ configuration is expected to be a coupled band with $B(M1)/B(E2)$ ratios $\sim 0.5\,(\mu_{\rm N}/{\rm eb})^2$ [16]. Hence, the $\pi g_{7/2}\otimes\pi(h_{11/2})^2$ configuration has been assigned for the decoupled band 4.

In the strongly coupled band 3, the lowest observed state has $J = 25/2$ at an excitation energy of 2973 keV. The band shows a small signature splitting $\Delta e' \sim 0$ keV and a large initial alignment $\sim 7\hbar$ implying a three-quasiparticle configuration also for this band. The alignment remains constant in the frequency range 0.30–0.45 MeV, indicating likely involvement of both the $\pi h_{11/2}$ and $\nu h_{11/2}$ quasiparticles in the configuration on the basis of blocking arguments. Moreover, since high-K strongly coupled bands based on the $\nu g_{7/2}\otimes\nu h_{11/2}$ configuration have systematically been observed in the even-even $^{124-128}$Xe [27–30] and $^{124-128}$Ba isotopes [25,31,32], the $\pi h_{11/2}\otimes\nu g_{7/2}\otimes\nu h_{11/2}$ configuration is proposed for band 3. Furthermore, the experimental $B(M1)/B(E2)$ ratios $\sim 2\,(\mu_{\rm N}/{\rm eb})^2$ extracted for band 3 are in agreement with the predicted ones. The calculations for the other possible configuration $\pi(g_{9/2})\otimes\pi(h_{11/2})^2$ suggested in ref. [9] yield low $B(M1)/B(E2)$ ratios $\sim 0.5\,(\mu_{\rm N}/{\rm eb})^2$ [16].

3.1 Total Routhian Surface calculations

The experimentally observed rotational structures in ^{123}Cs are discussed using Total Routhian Surface (TRS) formalism [33–35]. These calculations employed a triaxial Woods-Saxon single-particle potential [36] and a monopole pairing force residual interaction. The total Routhian is calculated in a self-consistent manner on a grid in deformation space, including quadrupole (β_2), hexadecapole (β_4) and triaxiality (γ) degrees of freedom, and then minimised with respect to the shape parameters to obtain equilibrium deformations. TRS maps calculated at $\hbar\omega = 0.24$ MeV are plotted in fig. 3(a-d). The labelling of the single-quasiparticle levels using the parity and signature notation is given in table 2. Average deformations for various configurations are summarised in table 3.

The calculations show that this nucleus is a well-deformed prolate rotor at low spins with γ being close to zero for the assigned configurations.

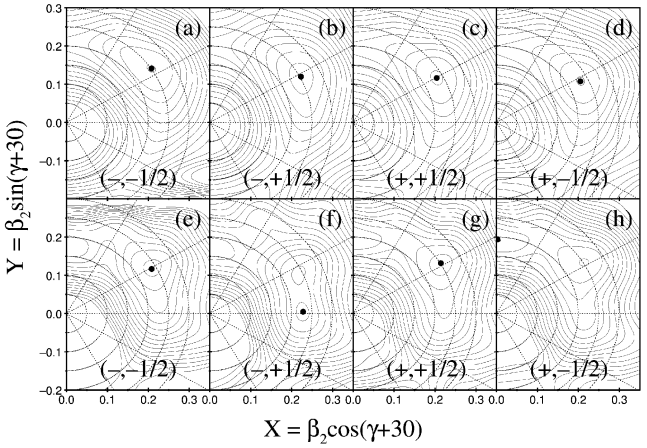

Fig. 3. Examples of TRS maps for configurations in ^{123}Cs. The energy contours are separated by 250 keV. Panels (a-d) are calculated at a frequency of 0.243 MeV/ω (spin $\sim 8\hbar$), while panels (e-h) are calculated at a frequency of 0.486 MeV/ω (spin $\sim 21\hbar$).

Table 2. Labelling of the single-quasiparticle levels.

Label	parity, signature	Nilsson orbital
E	$\pi(-,-1/2)$	$h_{11/2}[550]1/2^-$
F	$\pi(-,+1/2)$	$h_{11/2}[550]1/2^-$
A	$\pi(+,+1/2)_1$	$d_{5/2}[420]1/2^+$ (ground state)
B	$\pi(+,-1/2)_1$	$g_{7/2}[422]3/2^+$
C	$\pi(+,+1/2)_2$	$g_{9/2}[404]9/2^+$
D	$\pi(+,-1/2)_2$	$g_{9/2}[404]9/2^+$
E	$\nu(-,-1/2)$	$h_{11/2}[523]7/2^-$
F	$\nu(-,+1/2)$	$h_{11/2}[523]7/2^-$
B	$\nu(+,-1/2)$	$g_{7/2}[404]7/2^+$(or $d_{5/2}[402]5/2^+$)

Table 3. Assigned configurations and the average-deformation parameters.

Band	Configuration	β_2	β_4	Γ
1	E	0.250	0.006	4°
	F	0.250	0.005	−2°
2	E-γ			
5	C/D	0.230	0.000	−1°
6	A	0.230	0.002	0°
	B	0.230	0.000	−2°
3	Ebe	0.250	0.003	0°
4	BEFef	0.250	0.030	2°

Table 4. Single-particle energies of protons and neutrons.

Proton orbit	$p_{3/2}$	$p_{1/2}$	$f_{5/2}$	$g_{9/2}$	$g_{7/2}$	$d_{5/2}$	$d_{3/2}$	$s_{1/2}$	$h_{11/2}$
Energy (MeV)	−21.601	−20.501	−22.351	−18.251	−13.491	−14.051	−11.701	−12.071	−10.761
Neutron orbit	$p_{3/2}$	$p_{1/2}$	$f_{5/2}$	$g_{9/2}$	$g_{7/2}$	$d_{5/2}$	$d_{3/2}$	$s_{1/2}$	$h_{11/2}$
Energy (MeV)	−24.110	−23.010	−24.860	−20.760	−16.000	−16.560	−14.210	−14.580	−13.270

Although a stable prolate shape is predicted for ^{123}Cs at low spin, competing shapes become evident at higher spin, as shown in fig. 3(e-h). For example, the $(-,+1/2)$ configuration exhibits an energy minimum at $\gamma = -30^\circ$ (fig. 3(f)), while the $(+,-1/2)$ configuration exhibits a non-collective oblate minimum with $\gamma = +60^\circ$ (fig. 3(h)). Indeed a particularly favoured non-collective state at $J^\pi = 59/2^+$is expected in ^{123}Cs based on the aligned $\pi[g_{7/2}(h_{11/2})^2]^+_{27/2} \otimes \nu[(h_{11/2})^4]^+_{16}$ configuration.

3.2 Deformed Hartree-Fock and angular-momentum projection (PHF) calculations

The level energies and electromagnetic properties of the ^{123}Cs nucleus have been studied using deformed Hartree-Fock and angular-momentum projection (PHF) techniques. The formalism is discussed in [37,38]. The deformed HF equation is derived from a nuclear Hamiltonian. The surface delta interaction with interaction strength $V_{\rm pp} = V_{\rm np} = V_{\rm nn} = 0.315$ MeV is taken as the two-body interaction among the active nucleons (this is a reasonable interaction for this mass region and other complex nuclei [39]). Axial symmetry of the Hartree-Fock field is assumed. The deformed HF orbits are calculated with a spherical closed shell core with $Z = N = 28$.

The model space used for the HF orbits and angular-momentum–projected spectra calculations along with respective single-particle energies are given in table 4. Deformed HF orbits are obtained from a self-consistent solution of the HF equation [37,38].

Here a prolate HF solution is considered because it is lower in energy than the oblate solution. Prolate HF orbits for protons and neutrons (27 active protons and 40 neutrons) of ^{123}Cs are shown in fig. 4. One can get an intrinsic state $|\phi_K\rangle$ from the HF configuration by making an appropriate particle-hole arrangement near the proton and neutron Fermi surfaces. A given intrinsic state $|\phi_K\rangle$ does not have a unique angular-momentum quantum number and is a superposition of various J states, *i.e.*, $|\phi_K\rangle = \sum C^J_K |\psi_{JK}\rangle$ (because of axial symmetry of the deformed HF field, the basic intrinsic states are states of good K but not of good J). The state of a given angular momentum (J) is obtained by angular momentum projection formalism. The J projection operator is [37]

$$P^{JM}_K = \frac{2J+1}{8\pi^2} \int {\rm d}\Omega\, D^{J^*}_{MK}(\Omega)\, R(\Omega)\ , \qquad (1)$$

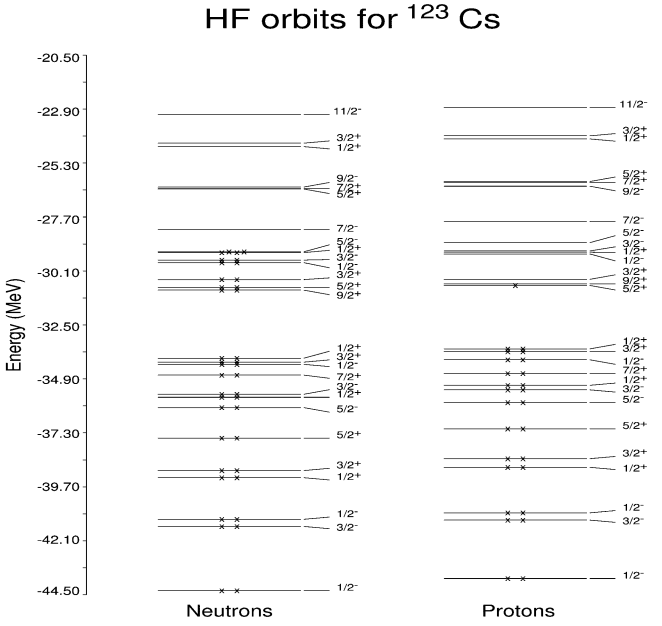

Fig. 4. The deformed prolate HF orbits with $Z = 55$ and $N = 68$ are shown. The orbits are denoted by J^π. Occupied orbits are denoted by (×).

where $R(\Omega)$ is the rotation operator and Ω stands for the Euler angles. The level energies can be obtained from the matrix element of the Hamiltonian between projected states of J obtained from intrinsic states $|\phi_{K1}\rangle$ and $|\phi_{K2}\rangle$, *viz*,

$$H^J_{K_1K_2} = \frac{2J+1}{2} \frac{1}{\left(N^J_{K_1K_1} N^J_{K_2K_2}\right)^{1/2}} \times \int_0^\pi {\rm d}\beta\, \sin(\beta)\, {\rm d}^J_{K_1K_2}(\beta)\, \left\langle \phi_{K_1} | H e^{-i\beta J_y} | \phi_{K2} \right\rangle . \quad (2)$$

Here

$$N^J_{K_1K_2} = \frac{2J+1}{2} \times \int_0^\pi {\rm d}\beta\ \sin(\beta)\, {\rm d}^J_{K_1K_2}(\beta) \left\langle \phi_{K_1} | e^{-i\beta J_y} | \phi_{K2} \right\rangle \qquad (3)$$

is the amplitude overlap for angular momentum J between the two intrinsic configurations $|\phi_{K1}\rangle$ and $|\phi_{K2}\rangle$.

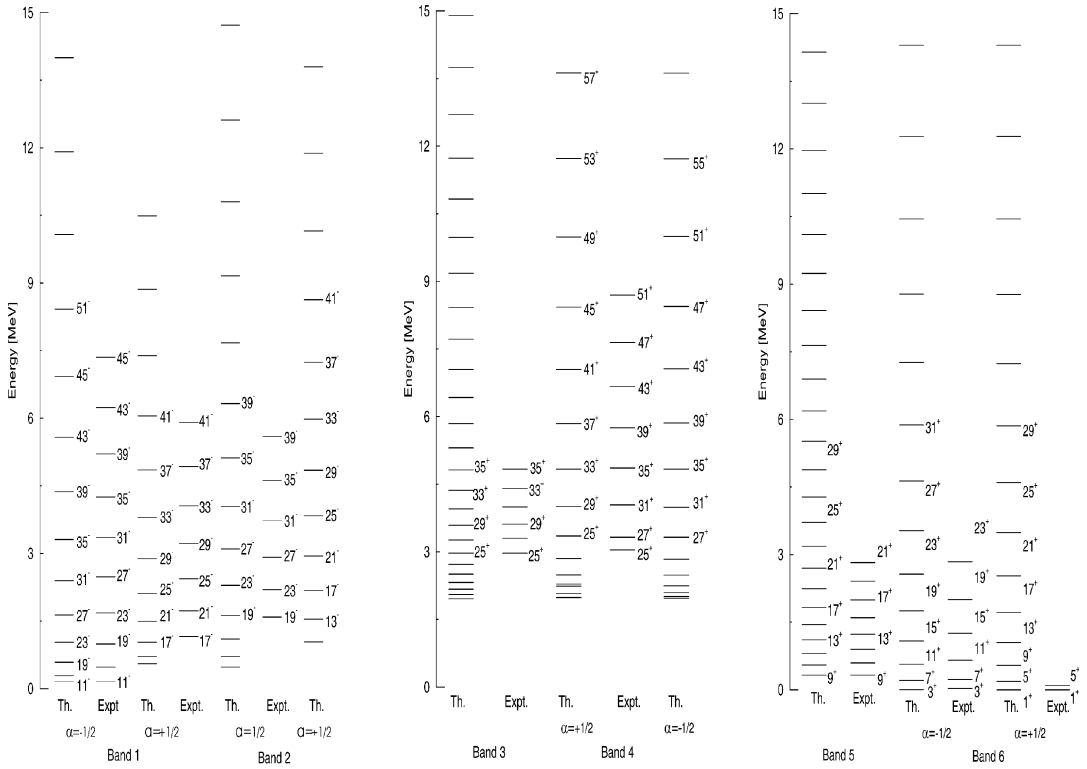

Fig. 5. Comparisons of PHF calculated level energies with the experiment for bands 1–6 in ^{123}Cs. Rotational states with $J = 11/2^-$, $19/2^-$, $9/2^+$, $1/2^+$, $25/2^+$ and $27/2^+$ are normalised for bands 1–6, respectively. The level spins shown are multiplied by 2.

The $B(E2)$ and $B(M1)$ values for the coupled bands are deduced from the reduced matrix elements of tensor operator T^L of rank L, denoting the electromagnetic operator ($E2$, $M1$ etc.), between projected states $\psi^{J_1}_{K1}$ and $\psi^{J_2}_{K2}$. These matrix elements are given by

$$\left\langle \psi^{J_1}_{K_1} \middle\| T^L \middle\| \psi^{J_2}_{K_2} \right\rangle = \frac{1}{2} \frac{(2J_2+1)\ (2J_1+1)^{1/2}}{\left(N^{J_1}_{K_1K_1} N^{J_2}_{K_2K_2}\right)^{1/2}} \times \sum_{\mu\nu} C^{J_2LJ_1}_{\mu\nu K_1} \int_0^\pi \mathrm{d}\beta\ \sin(\beta)\ \mathrm{d}^{J_2}_{\mu K_2}(\beta) \times \left\langle \phi_{K_1} \left| T^L_\nu e^{-i\beta J_y} \right| \phi_{K2} \right\rangle . \quad (4)$$

K_1, K_2 are axial quantum numbers. Effective charges of 1.45e for protons and 0.45e for neutrons are used to calculate $B(E2)$ values from reduced $E2$ matrix elements. g-factors $g_l = \mu_\mathrm{N}$ and $g_s = 1/2(-5.586)\,\mu_\mathrm{N}$ for protons and $g_l = 0$ and $g_s = 1/2(-3.826)\,\mu_\mathrm{N}$ for neutrons are used for calculating $B(M1)$ from reduced $M1$ matrix elements (quenching of spin g-factors is taken as half). For more details see ref. [40].

In general, two states $\left|\psi^{JM}_{K1}\right\rangle$ and $\left|\psi^{JM}_{K2}\right\rangle$ projected from two intrinsic configurations $|\phi_{K1}\rangle$ and $|\phi_{K2}\rangle$ are not orthogonal to each other, even if intrinsic states $|\phi_{K1}\rangle$ and $|\phi_{K2}\rangle$ are orthogonal (the rotation operator $e^{-i\beta J_y}$ in eqs. (2)–(4) can mix different intrinsic states. When necessary we orthonormalise using the following equation [38]:

$$\sum_{K'} \left(H^J_{KK'} - E_J N^J_{KK'}\right) C^J_{K'} = 0\,. \quad (5)$$

Here $C^J_{K'}$ are the orthonormalised amplitudes, which can be identified as the band-mixing amplitudes. It is established that the deformed HF and J projection in the form of band-mixing can give accurate results comparable to shell model diagonalisation [41].

We considered the following odd nucleon configurations on the respective time-reversal symmetric deformed cores and performed angular-momentum projection for the whole system, *i.e.*, odd nucleons ⊗ deformed core:
(a) $\pi h_{11/2}(1/2)$; $K^\pi = 1/2^-$,
(b) $\pi g_{9/2}(9/2)$; $K^\pi = 9/2^+$,
(c) $\pi g_{7/2}(1/2)$; $K^\pi = 1/2^+$,
(d) $\pi h_{11/2}(1/2) \otimes \nu h_{11/2}(7/2) \otimes \nu g_{7/2}(5/2)$; $K^\pi = 13/2^+$,
(e) $\pi g_{7/2}(1/2) \otimes \nu h_{11/2}(7/2) \otimes \nu h_{11/2}(-5/2)$; $K^\pi = 3/2^+$,
(f) $\pi h_{11/2}(3/2)$; $K^\pi = 3/2^-$,
(g) $\pi h_{11/2}(5/2)$; $K^\pi = 5/2^-$,
(h) $\pi g_{7/2}(1/2) \otimes \nu h_{11/2}(7/2) \otimes \nu h_{11/2}(-1/2)$; $K^\pi = 1/2^+$.

The number within parentheses indicates the Ω value for the time-reversal orbits. Referring to HF orbits in fig. 4, the $\pm 1/2^-$, $\pm 3/2^-$, $\pm 5/2^-$ orbits are near the proton Fermi surface and originate from the $h_{11/2}$ proton subshell and hence can show rotation alignment properties [42].

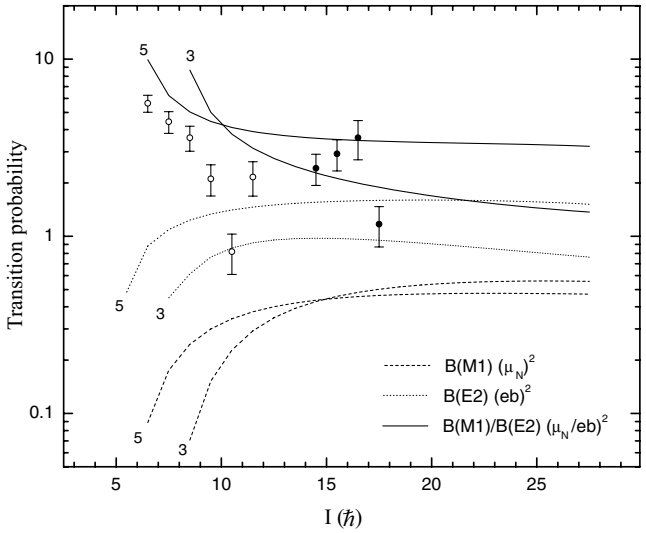

Fig. 6. The $M1$ and $E2$ transition probabilities and their ratios for the bands 3 and 5 calculated using the PHF model (shown as lines). Filled and open symbols represent the respective experimental ratios.

Configurations (f) and (g) originate from the odd proton $h_{11/2}$ orbit and are similar to configuration (a) and are thus (chiral) partner of (a). We have performed band-mixing calculation among the $\pi h_{11/2}$ bands with (a), (f) and (g) configurations. The lowest band after band-mixing is compared with level energies of band 1 and the first-excited band is compared with band 2 (fig. 5).

Configuration (c) for band 6 results in decoupled structure. In this case $\alpha = -1/2$ is the favoured branch, which is the same as experiment. For the $\alpha = +1/2$ signature branch, $J = 1/2^+$ is obtained as the lowest state and only $J = 1/2^+$ and $5/2^+$ states have been observed (fig. 5). For band 5, the calculated level energies for the odd proton configuration (b) are in agreement with the observed ones (fig. 5). For this band, $B(M1)/B(E2)$ values decrease smoothly from $9.9\,(\mu_{\rm N}/{\rm eb})^2$ for $J_i = 13/2$ and saturate at $\sim 3.4\,(\mu_{\rm N}/{\rm eb})^2$ for $J_i \sim 25/2$ and above (fig. 6). The observed values are also high $\sim 3.5\,(\mu_{\rm N}/{\rm eb})^2$. Band 3, which is a three-quasiparticle band, has been calculated with the configuration (d). We have also considered the $\pi g_{9/2}(9/2) \otimes \nu(h_{11/2})^2$ and $\pi h_{11/2}(1/2) \otimes \nu h_{11/2}(5/2) \otimes \nu d_{5/2}(5/2)$ configurations for comparison. The configuration (d) gives good agreement with experimental level spacings (fig. 5) and $B(M1)/B(E2)$ values for this band $\sim 2\,(\mu_{\rm N}/{\rm eb})^2$ (fig. 6). It is a high-K three-quasiparticle band.

Band-mixing calculations among the configurations (e) and (h) were performed. The lowest band after this band-mixing is compared with experimental band 4 and gives reasonable agreement (fig. 5). This configuration gives a bandhead energy of 3.825 MeV compared to the observed value of 3.331 MeV. Even the configuration (e) considered alone gives a bandhead energy of 4.325 MeV. The $\pi g_{7/2}(1/2) \otimes \pi h_{11/2}(+1/2) \otimes \pi h_{11/2}(-1/2)$ configuration favoured by the additivity of alignment and the observed upbend (fig. 2), probably due to the $(\nu h_{11/2})^2$ alignment, was also considered for comparison. The level spacings calculated for this configuration also compare reasonably well with the experiment, however, the calculated bandhead energy ~ 11.67 MeV is higher. The calculated $B(M1)/B(E2)$ values for both the configurations, *viz*, $\pi g_{7/2} \otimes \pi(h_{11/2})^2$ and $\pi g_{7/2} \otimes \nu(h_{11/2})^2$ configurations are rather low $\sim 0.1\,(\mu_{\rm N}/{\rm eb})^2$. The configurations assigned for the bands in ^{123}Cs on the basis of PHF calculations have been summarized in table 5.

Table 5. PHF configurations assigned for the bands in ^{123}Cs (configurations in square parentheses are used in band-mixing calculations).

Band	PHF configurations
1, 2	[(a), (f), (g)]
5	(b)
6	(c)
3	(d)
4	[(e), (h)]

4 Summary

Collective structures of the ^{123}Cs nucleus have been studied and assigned the Nilsson configurations. The bandhead excitation energies for the $\pi g_{7/2}$ and $\pi g_{9/2}$ bands have been established. The $\pi g_{9/2}$ bandhead is observed to be isomeric, which is consistent with the systematic of Cs and I isotopes. Theoretical description of the band structures of ^{123}Cs has been given in this paper. Total Routhian Surface (TRS) calculations were used to obtain the nuclear shape parameters (β_2, β_4, γ) for various configurations. Further calculations, based on deformed Hartree-Fock and angular-momentum projection from suitable intrinsic states and with two-body residual interaction among nucleons in a reasonable model space, have been used to study the observed band structures. Level energies and $B(M1)/B(E2)$ ratios have, on the whole, been reproduced for the assigned configurations based on low-lying intrinsic states of one and three unpaired nucleons.

The authors are thankful to the pelletron accelerator staff of the Nuclear Science Centre, New Delhi, for their excellent support during the experiment. Financial support from the UGC, New Delhi, under the Center of Advanced Study Funds, CSIR, New Delhi and the UK Engineering and Physical Sciences Research Council is acknowledged. The authors thank Drs R. Wyss and W. Nazarewicz for providing the TRS codes.

References

1. Y. Liang, R. Ma, E.S. Paul, N. Xu, D.B. Fossan, Phys. Rev. Lett. **64**, 29 (1990).
2. J. Dudek, K. Pomorski, N. Schunck, N. Dubray, Eur. Phys. J. A **20**, 15 (2004).

3. S. Zhu, U. Garg, B.K. Nayak, S.S. Ghugre, N.S. Pattabiraman, D.B. Fossan, T. Koike, K. Starosta, C. Vaman, R.V.F. Janssens, R.S. Chakrawarthy, M. Whitehead, A.O. Macchiavelli, S. Frauendorf, Phys. Rev. Lett. **91**, 132501 (2003).
4. E. Mergel, C.M. Petrache, G. Lo Bianco, H. Hübel, J. Domscheit, D. Roßbach, G. Schönwaßer, N. Nenoff, A. Neußer, A. Görgen, F. Becker, E. Bouchez, M. Houry, A. Hürstel, Y. Le Coz, R. Lucas, Ch. Theisen, W. Korten, A. Bracco, N. Blasi, F. Camera, S. Leoni, F. Hannachi, A. Lopez-Martens, M. Rejmund, D. Gassmann, P. Reiter, P.G. Thirolf, A. Astier, N. Buforn, M. Meyer, N. Redon, O. Stezowski, Eur. Phys. J. A **15**, 417 (2002).
5. R. Kumar, K. Singh, D. Mehta, N. Singh, S.S. Malik, E.S. Paul, A. Gorgen, S. Chmel, R.P. Singh, S. Muralithar, Eur. Phys. J. A **24**, 13 (2005).
6. G. Rainovski, E.S. Paul, H.J. Chantler, P.J. Nolan, D.G. Jenkins, R. Wadsworth, P. Raddon, A. Simons, D.B. Fossan, T. Koike, K. Starosta, C. Vaman, E. Farnea, A. Gadea, Th. Kroll, G. de Angelis, R. Isocrate, D. Curien, V.I. Dimitrov, J. Phys. G **29**, 2763 (2003).
7. C.W. Beausang, J. Simpson, J. Phys. G **22**, 527 (1996).
8. K. Singh, J. Goswamy, D. Mehta, N. Singh, R.P. Singh, S. Muralithar, E.S. Paul, K.P. Singh, N. Madhavan, J.J. Das, S. Nath, A. Jhingan, P. Sughathan, R.K. Bhowmik, Eur. Phys. J. A **21**, 359 (2004).
9. A.K. Singh, H. Hubel, J. Domsheit, G.B. Hagemann, B. Herskind, D.R. Jensen, J.N. Wilson, R. Clark, M. Cromaz, P. Fallon, A. Gorgen, I.Y. Lee, A.O. Macchiavelli, D. Ward, H. Amro, W.C. Ma, J. Timar, I. Ragnarsson, Phys. Rev. C **70**, 034315 (2004).
10. `http://www.nsc.ernet.in/research/nuclear_physics/`.
11. D.C. Radford, Nucl. Instrum. Methods A **361**, 297 (1995).
12. J. Singh, R. Singh, N. Singh, P.N. Trehan, in *Proceedings of DAE Symposium on Nuclear Physics, Utkal University, Bhubaneswar, India, 1994*, edited by R.K. Choudhury, A.K. Mohanty, Nucl. Phys. B (Proc. Suppl.) **37**, 455 (1994).
13. A. Gizon, B. Weiss, P. Paris, C.F. Liang, J. Genevey, J. Gizon, V. Barci, Gh. Cata-Danil, J.S. Dionisio, J.M. Lagrange, M. Pautrat, J. Vanhorenbeeck, Ch. Vieu, L. Zolnai, J.M. Arias, J. Barea, Ch. Droste, Eur. Phys. J. A **8**, 41 (2000).
14. G. Marguier, A. Charvet, J. Genevey, C. Richard-Serre, A. Knipper, G. Walter, the ISOLDE Collaboration, J. Phys. G **7**, 101 (1981)
15. J.R. Hughes, D.B. Fossan, D.R. LaFosse, Y. Liang, P. Vaska, M.P. Waring, J.-Y. Zhang, Phys. Rev. C **45**, 2177 (1992).
16. F. Lidén, B. Caderwall, P. Ahonen, D.W. Banes, B. Fant, J. Gascon, L. Hildingsson, A. Johnson, S. Juutinen, A. Kirwan, D.J.G. Love, S. Mitarai, J. Mukai, A.H. Nelson, J. Nyberg, J. Simpson, R. Wyss, Nucl. Phys. A **550**, 365 (1992).
17. S.M. Harris, Phys. Rev. **138**, 509B (1965).
18. L. Hildingsson, C.W. Beausang, D.B. Fossan, R. Ma, E.S. Paul, W.F. Piel jr., N. Xu, Phys. Rev. C **39**, 471 (1989).
19. J.F. Smith, V. Medina-Chico, C.J. Chiara, D.B. Fossan, G.J. Lane, J.M. Sears, I. Thorslund, H. Amro, C.N. Davids, R.V.F. Janssens, D. Seweryniak, I.M. Hibbert, R. Wadsworth, I.Y. Lee, A.O. Macchiavelli, Phys. Rev. C **63**, 024319 (2001).
20. D.J. Hartley, L.L. Riedinger, H.Q. Jin, W. Reviol, B.H. Smith, A. Galindo-Uribarri, D.G. Sarantites, D.R. LaFosse, J.N. Wilson, S.M. Mullins, Phys. Rev. C **60**, 014308 (1999).
21. J.R. Hughes, D.B. Fossan, D.R. LaFosse, Y. Liang, P. Vaska, M.P. Waring, Phys. Rev. C **44**, 2390 (1991).
22. Y. Liang, R. Ma, E.S. Paul, N. Xu, D.B. Fossan, Phys. Rev. C **42**, 890 (1990).
23. L. Hildingsson, W. Klamra, Th. Lindblad, F. Liden, Y. Liang, R. Ma, E.S. Paul, N. Xu, D.B. Fossan, J. Gascon, Z. Phys. A **340**, 29 (1991).
24. U. Garg, T.P. Sjoreen, D.B. Fossan, Phys. Rev. C **19**, 207 (1979).
25. S. Pilotte, S. Flibotte, S. Monaro, N. Nadon, D. Prévost, P. Taras, H. R. Andrews, D. Horn, V.P. Janzen, D.C. Radford, D. Ward, J.K. Johansson, J.C. Waddington, T.E. Drake, A. Galindo-Uribari, R. Wyss, Nucl. Phys. A **514**, 545 (1990).
26. H.I. Park, D.J. Hartley, L.L. Riedinger, W. Reviol, O. Zeidan, J.-Y. Zhang, A. Galindo-Uribarri, R.V.F. Janssens M.P. Carpenter, D. Seweryniak, D.G. Sarantites, M. Devlin, B.G. Dong, I. Ragnarsson, Phys. Rev. C **68**, 044323 (2003).
27. I. Schneider, R.S. Chakrawarthy, I. Wiedenhöver, A. Schmidt, H. Meise, P. Petkov, A. Dewald, P. von Brentano, O. Stuch, K. Jessen, D. Weisshaar, C. Schumacher, O. Vogel, G. Sletten, B. Herskind, M. Bergström, J. Wrzesinski, Phys. Rev. C **60**, 014312 (1999).
28. V. Werner, H. Meise, I. Wiedenhöver, A. Gade, P. von Brentano, Nucl. Phys. A **692**, 451 (2001).
29. W. Lieberz, S. Freund, A. Granderath, A. Gelberg, A. Dewald, R. Reinhardt, R. Wirowski, K.O. Zell, P. von Brentano, Z. Phys. A **330**, 221 (1988).
30. T. Lonnroth, S. Vajda, O.C. Kistner, M.H. Rafailovich, Z. Phys. A **317**, 215 (1984).
31. D. Ward, V.P. Janzen, H.R. Andrews, D.C. Radford, G.C. Ball, D. Horn, J.C. Waddington, J.K. Johansson, F. Banville, J. Gascon, S. Monaro, N. Nadon, S. Pilotte, D. Prevost, P. Taras, R. Wyss, Nucl. Phys. A **529**, 315 (1991).
32. O. Vogel, R.S. Chakrawarthy, A. Dewald, P. Petkov, K. Jessen, J. Gableske, P. von Brentano, D. Bazzacco, A. Gizon, J. Gizon, S. Lunardi, D.R. Napoli, P. Pavan, C. Rossi-Alvarez, I. Wiedenhöver, Eur. Phys. J. A **4**, 323 (1999).
33. W. Nazarewicz, G.A. Leander, J. Dudek, Nucl. Phys. A **467**, 437 (1987).
34. R. Wyss, J. Nyberg, A. Johnson, R. Bengtsson, W. Nazarewicz, Phys. Lett. B **215**, 211 (1988).
35. W. Nazarewicz, R. Wyss, A. Johnson, Nucl. Phys. A **503**, 285 (1989).
36. W. Nazarewicz, J. Dudek, R. Bengtsson, I. Ragnarsson, Nucl. Phys. A **435**, (1985) 397.
37. G. Ripka, *Advances in Nuclear Physics*, Vol. **1**, edited by M. Baranger, E. Vogt (Plenum, 1966).
38. C.R. Praharaj, J. Phys. G **14**, 843 (1988).
39. A. Faessler *et al.*, Phys. Rev. **156**, 1067 (1967).
40. Zashmir Naik, C.R. Praharaj, Phys. Rev. C **67**, 054318 (2003).
41. S.B. Khadkikar, S.C. Nair, S.P. Pandya, Phys. Lett. B **36**, 290 (1971).
42. F.S. Stephens, Rev. Mod. Phys. **47**, 43 (1975).